

Inverse Isotope Effect in the Ternary Perovskite Hydride SrPdH/D_{2.9}: A Signature of Quantum Zero-Point Fluctuations

Wencheng Lu,^{1,*} Mihir Sahoo,² Roman Lucrezi,³ Michael J. Hutcheon,⁴ Shubham Sinha,¹ Pedro N. Ferreira,² Chris J. Pickard,^{5,6} Qiang Zhang,⁷ Matthew N. Julian,⁴ Rohit P. Prasankumar,⁴ Christoph Heil,^{2,†} and Timothy A. Strobel^{1,‡}

¹*Earth and Planets Laboratory, Carnegie Institution for Science,
5241 Broad Branch Road NW, Washington, DC 20015, USA*

²*Institute of Theoretical and Computational Physics,
Graz University of Technology, NAWI Graz, 8010 Graz, Austria*

³*Department of Chemistry, Stockholm University, SE-10691 Stockholm, Sweden*

⁴*Enterprise Science Fund, Intellectual Ventures, 3150 139th Ave SE, Bellevue, WA, 98005, USA*

⁵*Department of Materials Science and Metallurgy, University of Cambridge,
27 Charles Babbage Road, Cambridge, CB3 0FS, UK*

⁶*Advanced Institute for Materials Research, Tohoku University, Sendai, 980-8577, Japan*

⁷*Neutron Scattering Division, Oak Ridge National Laboratory, Oak Ridge, TN, USA*

(Dated: March 2, 2026)

Guided by first-principles calculations, we demonstrate superconductivity in the ternary perovskite hydride SrPdH_{3-x}, synthesized at low pressure. Structural characterization via neutron diffraction reveals the near-stoichiometric composition SrPdD_{2.9(2)} with 96% deuterium site occupancy. Subsequent transport and magnetic susceptibility measurements establish onset superconducting transitions at $T_c = 2.1$ K (H) and $T_c = 2.2$ K (D), exhibiting an inverse isotope effect that our first-principles calculations attribute predominantly to quantum zero-point motion. The excellent agreement between theory and experiment with respect to thermodynamic stability and superconducting properties provides important validation for theory-guided superconductor discovery. This work establishes superconductivity in the perovskite hydride structural prototype—expanding the limited family of experimentally realized ternary hydride superconductors—and demonstrates the importance of quantum nuclear motion on the accurate theoretical treatment of low-pressure hydride superconductors.

The pursuit of high- T_c superconductivity in hydride systems has emerged as an active frontier in condensed matter physics. To date, realizing superconductivity at elevated temperatures in hydrides has required the application of extreme pressures. Most known high- T_c hydride superconductors fall within three well-established structural families: covalent hydrides (e.g., H₃S [1]), clathrate-type hydrides (e.g., LaH₁₀ [2], CaH₆ [3], and LaSc₂H₂₄ [4]), and molecular-type hydrides (e.g., BaH₁₂ [5], BiH₄ [6]). In an effort to lower the required synthetic pressure, substantial attention has been given to substitutional alloy hydrides [7], such as (La,Y)H₁₀ [8], (La,Ce)H₉ [9], and (Y,Ce)H₉ [10]. However, the substitutional alloying strategy often entails trade-offs between structural stability and the superconducting transition temperature. These hydrogen-rich structures generally demand high external pressure to stabilize dense hydrogen frameworks, significantly limiting their feasibility for ambient-pressure applications. Therefore, achieving superconductivity at high temperatures under reduced or ambient pressure remains a central and unresolved challenge, making the search for alternative structural prototypes increasingly important.

In recent studies, several ternary hydrides featuring unconventional structures have been successfully synthesized experimentally. These include the complex transition metal hydrides Li₅MoH₁₁ [11] and BaReH₉ [12], the fluorite-type hydride LaBeH₈ [13], and the lanthanum-based borohydride LaB₂H₈ [14]. However, these stoichiometric ternary compounds have also been found to be thermodynamically unstable at ambient pressure or to require high-pressure conditions to induce superconductivity.

Other structural families may also offer potential for superconductivity. Metals naturally possess interstitial sites capable of trapping hydrogen, leading to the formation of lower-hydrogen-content metallic hydrides [15]. These systems often exhibit favorable electronic structures and can remain stable at relatively low pressures (e.g., PdH with $T_c \approx 9$ K [16]). In such hydrides, hydrogen atoms are embedded within an electron-rich metallic matrix, enabling superconductivity without requiring extreme hydrogen ionization or ultrahigh pressure. Recent theoretical studies have also identified other candidates with high- T_c s under ambient or near-ambient pressures. These include complex transition-metal hydrides such as Mg₂IrH₆ (65–170 K) [17–20], perovskite hydrides exemplified by KInH₃ (73 K) [21], and anti-perovskite hydrides like ZnHAl₃ (80 K) [22]. Recent low-pressure studies in the Mg–Pt–H system revealed superconductivity in the novel complex hydride Mg₄Pt₃H₆ [23].

* wlu@carnegiescience.edu

† christoph.heil@tugraz.at

‡ tstrobel@carnegiescience.edu

Perovskite hydrides, characterized by a three-dimensional framework with A- and B-site cations and corner-sharing hydride octahedra (Fig. 1(a)), are fundamentally different to other high- T_c hydride prototypes. Unlike covalent or molecular hydrides, these materials exhibit hydridic bonding, which enhances metallicity and may facilitate superconducting pairing. Given their structural versatility, promising low-pressure thermodynamic stability, and high predicted T_c s, perovskite-type hydrides stand out as a compelling subclass in the search for practical high- T_c superconductors. Numerous compounds have been proposed as promising candidates exhibiting high T_c s at ambient conditions. Examples include RbPH_3 [24], KM_3H_3 with $M = \text{Al}$ (52 K), Cd (23.4 K) [25], [26]), MScH_3 [27] with $M = \text{K}$ (40.4 K), Rb (32.9 K), Cs (18.6 K), SrMH_3 [28] with $M = \text{Au}$ (132 K), Tc (69 K), Zn (107 K), Al_4H (54 K) [29], PbMH_3 [21] with $M = \text{Hg}$ (25.8 K), Os (23.2 K), Al-HgH_3 (28.4 K) [21]. Furthermore, Du *et al.* proposed five perovskite hydrides with T_c s exceeding 120 K under 10 GPa [30], KGaH_3 (146 K), RbInH_3 (130 K), CsInH_3 (153 K), RbTiH_3 (170 K), and CsTiH_3 (163 K). Despite the growing body of computational studies exploring superconductivity in this class of hydrides, the potential of this structure type remains unverified by experiment. The absence of direct experimental confirmation leaves a critical gap between theoretical predictions and practical realization, underscoring the need for targeted synthesis and characterization efforts.

In this work, we report the synthesis and characterization of SrPdH_{3-x} , a cubic perovskite superconductor that provides new insights into the physics of hydride superconductors. Using high-throughput computational screening, we identified this material as thermodynamically stable under ambient pressure. Subsequently, we were able to synthesize SrPdH_{3-x} under moderate conditions (560 bar, 475 °C), achieving the near-stoichiometric composition $\text{SrPdD}_{2.9(2)}$, as confirmed by neutron diffraction. Notably, our electrical transport and magnetic susceptibility measurements reveal an inverse isotope effect: deuterated samples exhibit slightly higher superconducting transition temperatures compared to their hydrogenated counterparts. Through state-of-the-art first-principles calculations combining density functional perturbation theory (DFPT) [31] with the stochastic self-consistent harmonic approximation (SSCHA) [32, 33], we demonstrate that this behavior arises from quantum nuclear effects. Our results provide the first quantitatively accurate theoretical reproduction of the inverse isotope effect in a ternary hydride superconductor, revealing fundamental physics that will be important for understanding and designing ambient-pressure superconducting hydrides.

As illustrated in the thermodynamic convex hull (Fig. 1(b)), our high-throughput calculations identify four thermodynamically stable ternary hydrides in the Pd–Sr–H system at ambient pressure: SrPdH_3 , Sr_2PdH_4 , Sr_2PdH_6 , and $\text{Sr}_4\text{Pd}_3\text{H}_6$. Among these, our initial coarse

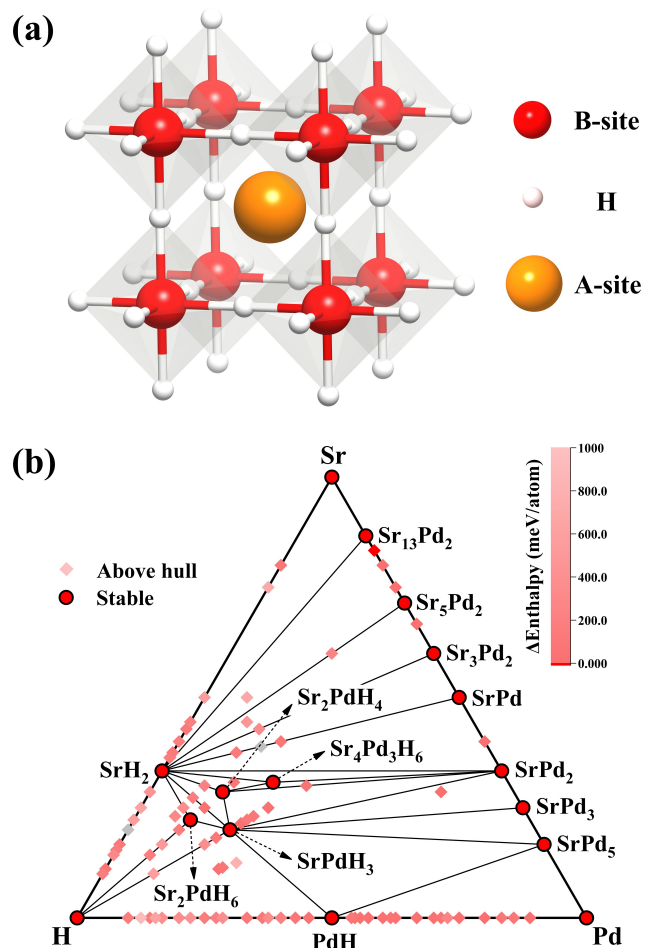


FIG. 1. **a** Crystal structure of perovskite hydrides, where the A-site, B-site and H atoms are shown as orange, red, and white spheres. In SrPdH_3 , Pd and Sr occupy the B-site and A-site, respectively. **b** Calculated ternary phase diagram of the Sr–Pd–H system at ambient pressure. Structures are represented by rhombuses and colored according to their distance from the convex hull; thermodynamically stable structures are indicated by red solid circles.

screening identified SrPdH_3 to be dynamically stable and to exhibit electron-phonon coupling, later refined to give a T_c of approximately 2.8 K through high-accuracy calculations described below.

To the best of our knowledge, Sr_2PdH_6 and $\text{Sr}_4\text{Pd}_3\text{H}_6$ remain unreported in prior experimental or theoretical studies. Their absence in experiments may be attributed to finite temperature effects or large kinetic barriers, potentially requiring alternative synthetic approaches. Synthesis of Sr_2PdH_4 , which adopts an orthorhombic crystal structure and exhibits insulating behavior, was reported in previous studies [34, 35], including both hydrogenated and deuterated forms.

SrPdH_{3-x} was previously synthesized by Bronger and Ridder in the 1990s [36], though our theoretical prediction and synthesis were conducted independently of this

earlier work. This phase crystallizes in the perovskite-type framework, where Sr atoms occupy the A-sites, and Pd atoms located at the B-sites are octahedrally coordinated by six hydrogen atoms that reside at the $3d$ Wyckoff positions and exhibit $4/m\bar{m}m$ site symmetry. Previous neutron diffraction measurements on samples synthesized at 5 bar indicated a composition of $\text{SrPdH}_{2.7}$, and the material was described as having a metallic copper-like appearance, though no physical properties were reported [36]. Later, Yagyū *et al.* prepared SrPdH_{3-x} with unidentified impurities using CaH_2 as the hydrogen source at ~ 5 bar and room temperature [37]. Based on magnetic susceptibility measurements, no superconducting transition was observed above 2 K.

Following our independent predictions, we attempted synthesis of SrPdH_3 by hydrogenating SrPd [38] (see Fig. S1) under relatively moderate conditions of 560 bar and 475°C (More details on the experimental and theoretical methods in Supplemental Information and Refs. [39–59]). After hydrogenation/ deuteration, the copper-colored product remains stable at ambient pressure (Fig. 2(a), inset), but decomposes in air and must be handled in an inert environment. In order to verify the crystal structure of the synthesized compound, powder XRD measurements were conducted at ambient pressure, as shown in Fig. 2(a). Rietveld analysis of the diffraction patterns indicate the formation of the SrPdH_{3-x} perovskite framework ($Pm\bar{3}m$) with minor Sr_2PdH_4 and SrO impurities. The experimental lattice parameter $a = 3.839(3)$ Å is in excellent agreement with the predicted theoretical value $a = 3.848$ Å — a difference of only 0.23%.

To determine the hydrogen content of the synthesized material, deuterated samples were prepared under the same conditions and analyzed using neutron powder diffraction. Rietveld refinement of the diffraction pattern obtained at 10 K (Fig. 2(b), with $a = 3.821(8)$ Å) yields the composition $\text{SrPdD}_{2.9(2)}$, showing higher deuterium content than reported previously [36]. This deviation is presumably due to the higher synthesis pressure used in this study (560 bar) compared to the 5 bar pressure used in earlier work.

The potential for superconductivity was investigated by performing electrical transport measurements with the assistance of a Quantum Design Physical Property Measurement System (PPMS, Model 6000). Representative temperature-dependent electrical transport data are presented in Fig. 3(a). Samples exhibit metallic conductivity with a clear superconducting transition characterized by a sharp drop to zero resistance for both the hydrogenated and deuterated samples. The superconducting onset temperature, T_c^{onset} , established by extrapolating the linear portions of the resistance curves immediately above and below the transition, was determined to be 2.1 K for the hydrogenated sample. Strikingly, deuterated samples exhibit a slightly enhanced T_c^{onset} of 2.2 K. This anomalous increase, opposite to the suppression anticipated within the conventional BCS framework [60], constitutes clear evidence of an *inverse isotope*

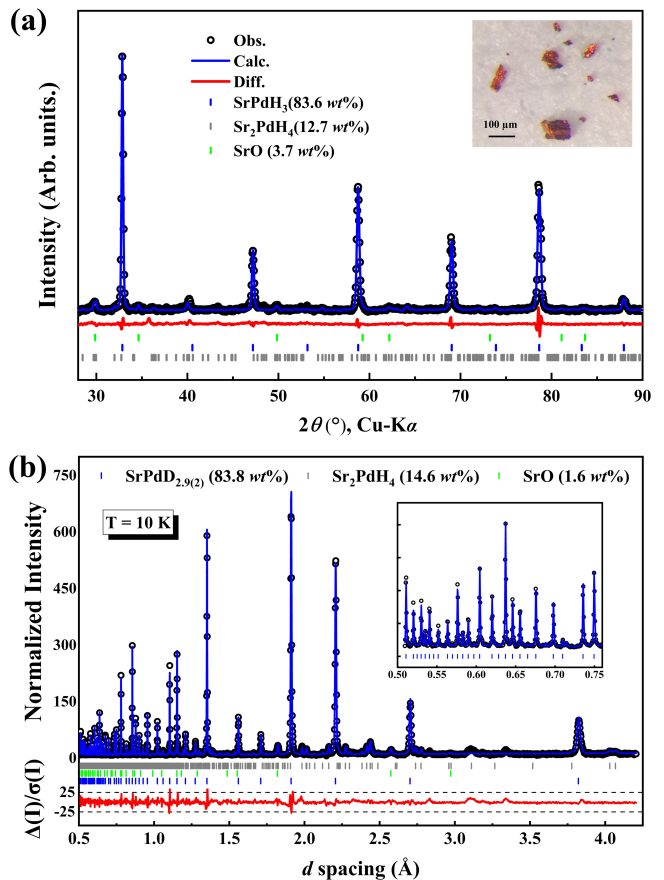


FIG. 2. **a** XRD pattern (black points) for hydrogenated samples (measured at room temperature) with Rietveld refinement ($R_{wp} = 4.89\%$) of the predicted $Pm\bar{3}m$ SrPdH_3 structure (blue line). The red line shows the Rietveld residual and vertical ticks marks indicate allowed Bragg reflections. Impurity peaks from SrO and Sr_2PdH_4 are represented by green and grey ticks, respectively. Inset: photographs of the sample after hydrogenation. **b** TOF-neutron diffraction pattern for deuterated sample at 10 K (black points) and Rietveld refinement (blue line) with R_{wp} of 8.17%. The red line shows the Rietveld residual and the vertical ticks mark the positions of nuclear peaks for $\text{SrPdD}_{2.9(2)}$ (blue), SrO (green) and Sr_2PdD_4 (grey).

effect. This counterintuitive behavior highlights anomalous aspects of the superconducting mechanism in these hydrides and will be revisited in detail below.

To further probe superconductivity, magnetic fields up to 0.05 T were applied during electrical transport measurements to investigate the upper critical field (as shown for the deuterated sample in Fig. 3(b) and hydrogenated sample in Fig. S3). The observed resistance drop exhibits systematic suppression with increasing field, further confirming the superconducting nature of the transition. To estimate the upper critical field, H_{c2} , the observed field-dependent transition temperatures were fitted to a modified Ginzburg–Landau (GL) expression, $H_{c2}(T) = H_{c2}(0)(1 - (T/T_c)^2)$, where $H_{c2}(T)$ is the up-

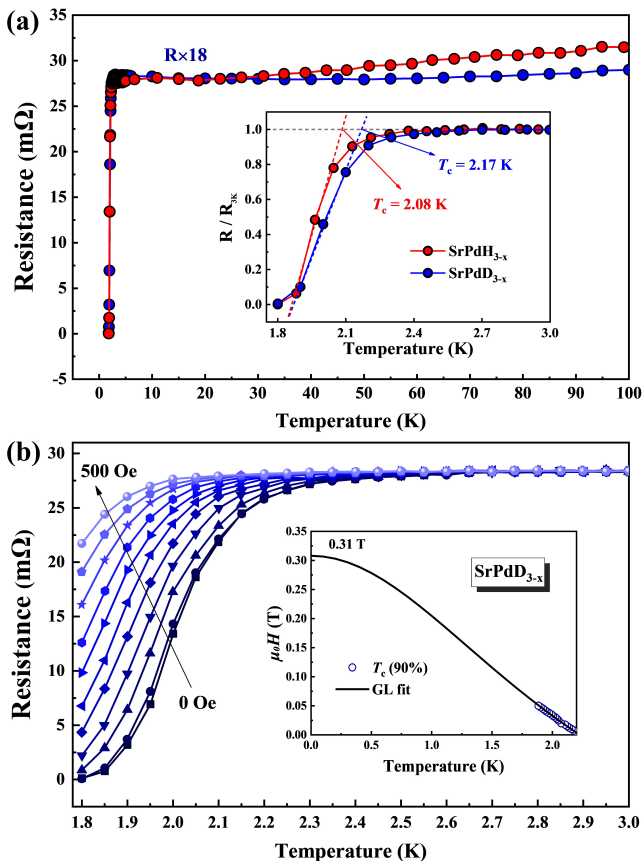


FIG. 3. **a** Electrical transport measurements of the synthesized hydride and deuteride under ambient pressure. Inset show the T_c^{onset} by extrapolating the linear portions of the resistance curves. **b** Temperature dependence of the electrical resistance for deuteride under applied magnetic fields up to 500 Oe, measured in steps of 50 Oe. The inset shows the GL fit and estimation of the upper critical field.

per critical field at temperature T , using the criterion of 90% of the normal-state resistance at 3 K to define T_c . From this analysis, we estimate a zero-temperature value of $\mu_0 H_{c2}(0) = 0.31$ T of deuterated sample.

To further confirm the superconducting nature of the transition observed by electrical transport, temperature-dependent AC magnetic susceptibility measurements were performed on H- and D-bearing samples using the ACSM-I option of the PPMS (see Supplementary Information). In both cases, samples clearly show magnetic field expulsion with a sharp drop in the real component of the susceptibility (χ'), signaling a diamagnetic transition, as well as energy dissipation with a rise in the imaginary component of the susceptibility (χ''). These observations confirm the superconducting nature of the samples and corroborate the observation from transport that T_c^{onset} for SrPdD_{3-x} is higher than that of SrPdH_{3-x} (Fig. S4).

To obtain a comprehensive theoretical understanding of the superconducting properties of these compounds, we performed additional high-accuracy calcu-

lations. We computed electron-phonon ($el-ph$) matrix elements on dense grids using DFPT as implemented in Quantum ESPRESSO [40], followed by Wannier interpolation via EPW to achieve even denser Brillouin zone (BZ) sampling [58, 61]. This approach ensures full convergence of the BZ integrals required for computing the Eliashberg spectral function $\alpha^2 F(\omega)$ [62, 63], which serves as the primary input for the Eliashberg equations to estimate T_c from first principles [64, 65]. The spectral function also enables calculation of two key parameters that characterize conventional superconductors [66]: the total $el-ph$ coupling strength $\lambda = \int \frac{d\omega}{\omega} \alpha^2 F(\omega)$ and the $el-ph$ -weighted averaged frequency $\omega_{\text{log}} = \exp \left[\frac{2}{\lambda} \int d\omega \frac{\ln(\omega)}{\omega} \alpha^2 F(\omega) \right]$.

Our calculations yield $\lambda = 0.4$ for both hydrogen and deuterium compounds, but reveal a larger $el-ph$ -weighted averaged frequency ω_{log} of 57 meV for SrPdH₃ compared to 43 meV for SrPdD₃, reflecting the higher vibrational frequencies of the lighter hydrogen atoms. Consequently, SrPdH₃ exhibits a slightly higher T_c of 2.8 K compared to 2.1 K for SrPdD₃, using the McMillan-Allen-Dynes formula [66] and the commonly adopted value $\mu_{\text{AD}}^* = 0.1$ for the Morel-Anderson Coulomb pseudopotential [67] in place of a full first-principles evaluation [64]. While these numerical T_c values closely match experimental results, they fail to reproduce the experimentally observed inverse isotope effect.

This is to be expected, as the above described workflow neglects quantum ionic anharmonic effects, which can be significant for compounds containing very light elements. In order to account for these effects, we employed the stochastic self-consistent harmonic approximation (SSCHA) with *ab initio*-trained machine learning potentials [54, 55], a cutting-edge approach that has only recently become computationally feasible for complex superconducting systems. In particular, we developed highly accurate interatomic potentials from our DFT data and utilized them to fully converge the SSCHA calculations, following the methodology outlined in Refs. [56, 57].

These calculations reveal that SrPdH₃ requires a larger equilibrium volume than SrPdD₃, which can be attributed to the larger zero-point motion displacements of hydrogen compared to deuterium. Expressing the same point from a different perspective: when SSCHA calculations are performed on structures relaxed within the Born-Oppenheimer approximation, they generate internal pressures of 2.1 GPa for SrPdH₃ and 1.6 GPa for SrPdD₃.

The volume expansion induces sizable shifts in the phonon spectrum, as can be appreciated in Fig. 4(a), which reduce the superconducting parameters of SrPdH₃ to $\lambda = 0.36$ and $\omega_{\text{log}} = 55$ meV, compared with $\lambda = 0.37$ and $\omega_{\text{log}} = 41$ meV for SrPdD₃. Eliashberg calculations using IsoME [64] give T_c values between 1.2 and 2.0 K, depending on μ^* [Fig. 4(b)], in excellent agreement with experiment. Moreover, for $\mu^* > 0.1$, the calculated T_c

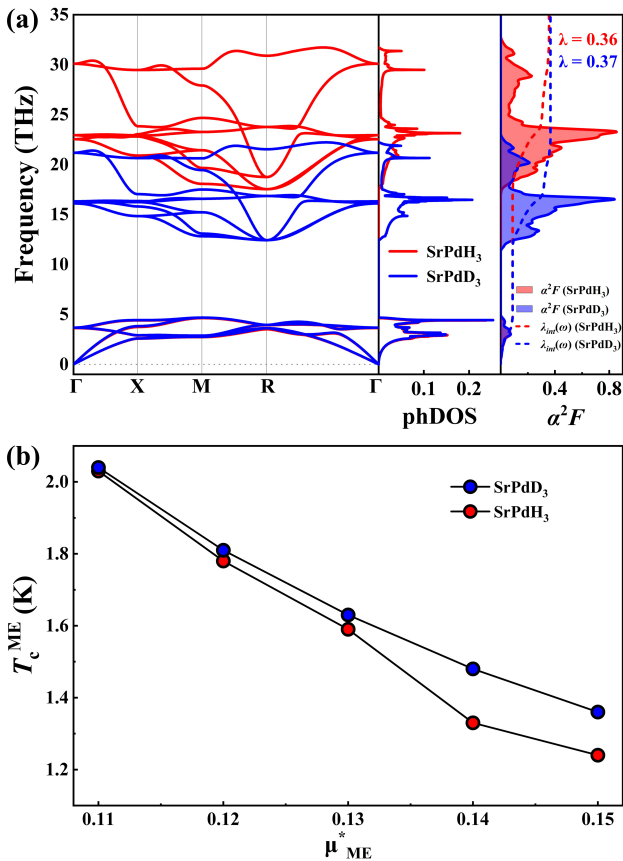


FIG. 4. **a** Anharmonic phonon dispersion, phonon DOS, Eliashberg spectral function $\alpha^2F(\omega)$, and cumulative $el-ph$ coupling $\lambda(\omega)$. **b** Critical temperatures determined via Migdal-Eliashberg theory as a function of screened Coulomb pseudopotential μ^* .

of SrPdD₃ consistently exceeds that of SrPdH₃, thereby reproducing the experimentally observed inverse isotope effect. The measured isotope coefficient of $\alpha \approx -0.07$ is accurately reproduced within the numerical precision of our calculations, confirming that the anomalous isotope dependence originates from the anharmonic volume expansion.

Further analysis reveals that anharmonicity in its strictest sense (non-parabolicity of the potential energy surface) and phonon-phonon interactions have minimal impact on the phonon and $el-ph$ properties. This highlights a fundamentally different mechanism for the inverse isotope effect compared to the extensively studied binary PdH(D) system [16, 68]. While Errea *et al.* [69] demonstrated that anharmonic effects in PdH arise from double-well potentials that stabilize otherwise unstable harmonic phonons, the situation in SrPdH₃ is markedly different. Here, the harmonic phonons are already stable and yield excellent agreement with experimental T_c values. Instead, the inverse isotope effect emerges predominantly from zero-point motion differences between H and D isotopes, which drive volume adjustments that

shift the phonon dispersion without requiring phonon-phonon interactions or potential anharmonicity.

Importantly, we propose that this quantum zero-point mechanism becomes progressively weaker at higher pressures, where increased structural rigidity suppresses volume expansion effects [56]. This pressure dependence provides a natural explanation for why high-pressure superconductors such as H₃S and LaH₁₀ exhibit conventional isotope effects rather than the inverse behavior observed here [1, 2], although structure-specific anharmonic effects are also relevant. These insights are therefore particularly significant for the ongoing search for higher- T_c ambient and low-pressure hydride superconductors, where accurate theoretical predictions require explicit treatment of quantum nuclear motion to capture isotope-dependent volume effects.

Finally, we discuss potential impacts related to compositional variability. While H- and D-bearing samples were synthesized under the same experimental conditions, we cannot explicitly rule out minor compositional variations that might contribute to differences in observed T_c s. Our calculations within the Generalized Quasichemical Approximation (GQCA) [59] incorporating hydrogen and deuterium vacancies (see SI for details) indicate that the density of states around the Fermi level remains almost unchanged for low vacancy concentrations (Fig. S5), and T_c is therefore expected to remain approximately constant across small changes in composition. Across all of our experiments, the observed T_c onset temperature was always higher for D samples than for H samples. These observations suggest that the systematic shift between H and D is robust with an origin rooted in zero-point nuclear quantum motion. Indeed, recent computational studies highlight the importance of anharmonic effects within the perovskite hydride structural prototype [24]. SrPdD/H_{3-x} thus appears to be the second known example of the inverse isotope effect in hydride superconductors. While previous measurements on SrPdH_{3-x} did not observe a superconducting transition [37], susceptibility measurements were only performed to 2 K, which may not be sufficiently low temperature to observe an unambiguous transition near the onset temperature for the hydride while screening.

In summary, we establish superconductivity in the perovskite hydride structural prototype using SrPdH/D_{3-x}, which represents a promising framework for hydride superconductors. Experimental measurements and theoretical calculations show that deuterated samples exhibit an anomalously higher T_c^{onset} (2.2 K) compared with hydrogenated samples (2.1 K), showing clear evidence of inverse-isotope-dependent behavior. By highlighting the essential role of quantum nuclear effects, our results broaden the scope for exploring anomalous superconductivity in complex hydrides and provide a framework for extending research possibilities to other low-pressure, hydrogen-rich materials.

ACKNOWLEDGMENTS

This work used the Spallation Neutron Source (SNS), a DOE Office of Science User Facility operated by the Oak Ridge National Laboratory. The beam time was allocated to Powgen BL-11A under proposal number IPTS-32521.1. The research was supported by the Enterprise

Science Fund of Intellectual Ventures. Computations were performed on the ICluster at TU Graz and the Austrian Scientific Computing clusters VSC4 and VSC5. R.L. acknowledges the Carl Tryggers Stiftelse för Vetenskaplig Forskning (CTS 23: 2934). PNF acknowledges support from the Austrian Science Fund (FWF) under project DOI 10.55776/ESP8588124.

-
- [1] A. Drozdov, M. Erements, I. Troyan, V. Ksenofontov, and S. I. Shylin, Conventional superconductivity at 203 kelvin at high pressures in the sulfur hydride system, *Nature* **525**, 73 (2015).
- [2] A. Drozdov, P. Kong, V. Minkov, S. Besedin, M. Kuzovnikov, S. Mozaffari, L. Balicas, F. F. Balakirev, D. Graf, V. Prakapenka, *et al.*, Superconductivity at 250 K in lanthanum hydride under high pressures, *Nature* **569**, 528 (2019).
- [3] L. Ma, K. Wang, Y. Xie, X. Yang, Y. Wang, M. Zhou, H. Liu, X. Yu, Y. Zhao, H. Wang, *et al.*, High-temperature superconducting phase in clathrate calcium hydride CaH_6 up to 215 K at a pressure of 172 GPa, *Phys. Rev. Lett.* **128**, 167001 (2022).
- [4] Y. Song, C. Ma, H. Wang, M. Zhou, Y. Qi, W. Cao, S. Li, H. Liu, G. Liu, and Y. Ma, Room-Temperature Superconductivity at 298 K in Ternary La-Sc-H System at High-pressure Conditions (2025), arXiv:2510.01273 [cond-mat.supr-con].
- [5] W. Chen, D. V. Semenok, A. G. Kvashnin, X. Huang, I. A. Kruglov, M. Galasso, H. Song, D. Duan, A. F. Goncharov, V. B. Prakapenka, *et al.*, Synthesis of molecular metallic barium superhydride: pseudocubic BaH_{12} , *Nature Commun.* **12**, 273 (2021).
- [6] P. Shan, L. Ma, X. Yang, M. Li, Z. Liu, J. Hou, S. Jiang, L. Zhang, L. Shi, P. Yang, *et al.*, Molecular Hydride Superconductor BiH_4 with T_c up to 91 K at 170 GPa, *J. Am. Chem. Soc.* **147**, 4375 (2024).
- [7] D. V. Semenok, D. Zhou, W. Chen, A. G. Kvashnin, A. V. Sadakov, T. Helm, P. N. Ferreira, C. Heil, V. M. Pudalov, I. A. Troyan, and V. V. Struzhkin, Stability and Superconductivity of Ternary Polyhydrides (2025), arXiv:2509.22877 [cond-mat.supr-con].
- [8] D. V. Semenok, I. A. Troyan, A. G. Ivanova, A. G. Kvashnin, I. A. Kruglov, M. Hanfland, A. V. Sadakov, O. A. Sobolevskiy, K. S. Pervakov, I. S. Lyubutin, *et al.*, Superconductivity at 253 K in lanthanum-yttrium ternary hydrides, *Mater. Today* **48**, 18 (2021).
- [9] J. Bi, Y. Nakamoto, P. Zhang, K. Shimizu, B. Zou, H. Liu, M. Zhou, G. Liu, H. Wang, and Y. Ma, Giant enhancement of superconducting critical temperature in substitutional alloy $(\text{La,Ce})\text{H}_9$, *Nature Commun.* **13**, 5952 (2022).
- [10] L.-C. Chen, T. Luo, Z.-Y. Cao, P. Dalladay-Simpson, G. Huang, D. Peng, L.-L. Zhang, F. A. Gorelli, G.-H. Zhong, H.-Q. Lin, *et al.*, Synthesis and superconductivity in yttrium-cerium hydrides at high pressures, *Nature Commun.* **15**, 1809 (2024).
- [11] D. Meng, M. Sakata, K. Shimizu, Y. Iijima, H. Saitoh, T. Sato, S. Takagi, and S.-i. Orimo, Superconductivity of the hydrogen-rich metal hydride $\text{Li}_5\text{MoH}_{11}$ under high pressure, *Phys. Rev. B* **99**, 024508 (2019).
- [12] T. Muramatsu, W. K. Wanene, M. Somayazulu, E. Vinitzky, D. Chandra, T. A. Strobel, V. V. Struzhkin, and R. J. Hemley, Metallization and superconductivity in the hydrogen-rich ionic salt BaReH_9 , *J. Phys. Chem. C* **119**, 18007 (2015).
- [13] Y. Song, J. Bi, Y. Nakamoto, K. Shimizu, H. Liu, B. Zou, G. Liu, H. Wang, and Y. Ma, Stoichiometric ternary superhydride LaBeH_8 as a new template for high-temperature superconductivity at 110 K under 80 GPa, *Phys. Rev. Lett.* **130**, 266001 (2023).
- [14] X. Song, X. Hao, X. Wei, X.-L. He, H. Liu, L. Ma, G. Liu, H. Wang, J. Niu, S. Wang, *et al.*, Superconductivity above 105 K in nonclathrate ternary lanthanum borohydride below megabar pressure, *J. Am. Chem. Soc.* **146**, 13797 (2024).
- [15] H. J. Goldschmidt, Hydrides, in *Interstitial Alloys* (Springer US, Boston, MA, 1967) pp. 445–531.
- [16] B. Stritzker and W. Buckel, Superconductivity in the palladium-hydrogen and the palladium-deuterium systems, *Z. Phys. A* **257**, 1 (1972).
- [17] K. Dolui, L. J. Conway, C. Heil, T. A. Strobel, R. P. Prasankumar, and C. J. Pickard, Feasible route to high-temperature ambient-pressure hydride superconductivity, *Phys. Rev. Lett.* **132**, 166001 (2024).
- [18] A. Sanna, T. F. Cerqueira, Y.-W. Fang, I. Errea, A. Ludwig, and M. A. Marques, Prediction of ambient pressure conventional superconductivity above 80 K in hydride compounds, *npj Comput. Mater.* **10**, 44 (2024).
- [19] F. Zheng, Z. Zhang, Z. Wu, S. Wu, Q. Lin, R. Wang, Y. Fang, C.-Z. Wang, V. Antropov, Y. Sun, *et al.*, Prediction of ambient pressure superconductivity in cubic ternary hydrides with MH_6 octahedra, *Mater. Today Phys.* **42**, 101374 (2024).
- [20] M. F. Hansen, L. J. Conway, K. Dolui, C. Heil, C. J. Pickard, A. Pakhomova, M. Mezouar, M. Kunz, R. P. Prasankumar, and T. A. Strobel, Synthesis of Mg_2ItH_5 : A potential pathway to high- T_c hydride superconductivity at ambient pressure, *Phys. Rev. B* **110**, 214513 (2024).
- [21] T. F. Cerqueira, Y.-W. Fang, I. Errea, A. Sanna, and M. A. Marques, Searching materials space for hydride superconductors at ambient pressure, *Adv. Funct. Mater.* **34**, 2404043 (2024).
- [22] S.-m. Liu, J.-j. Shi, Y. He, C. Tian, Y.-h. Zhu, X. Wang, and H.-x. Zhong, High-Throughput Study of Ambient-Pressure High-Temperature Superconductivity in Ductile Few-Hydrogen Metal-Bonded Perovskites, *Adv. Funct. Mater.* **34**, 2315386 (2024).
- [23] W. Lu, M. J. Hutcheon, M. F. Hansen, K. Dolui, S. Sinha, M. R. Sahoo, C. J. Pickard, C. Heil, A. Pakhomova, M. Mezouar, D. Daisenberger, S. Chariton, V. Prakapenka, M. N. Julian, R. P. Prasankumar, and T. A. Strobel, Prediction and synthesis of $\text{Mg}_4\text{Pt}_3\text{H}_6$: A

- superconducting complex transition metal hydride stabilized at ambient pressure, *Phys. Rev. B* **112**, 094513 (2025).
- [24] Dorđe Dangić, Y.-W. Fang, T. F. Cerqueira, A. Sanna, T. Novoa, H. Gao, M. A. Marques, and I. Errea, Ambient pressure high temperature superconductivity in RbPH3 facilitated by ionic anharmonicity, *Comput. Mater. Today* **8**, 100043 (2025).
- [25] D. Wines and K. Choudhary, Data-driven design of high pressure hydride superconductors using DFT and deep learning, *Mater. Futures* **3**, 025602 (2024).
- [26] T. F. Cerqueira, A. Sanna, and M. A. Marques, Sampling the materials space for conventional superconducting compounds, *Adv. Mater.* **36**, 2307085 (2024).
- [27] H. Quan, X.-B. Shi, Y.-L. Han, P. Zhang, and B.-T. Wang, Prediction of ambient-pressure superconductivity in the perovskite hydrides MScH_3 ($M = \text{K, Rb, Cs}$), *Phys. Rev. B* **111**, 134509 (2025).
- [28] B. Li, C. Zhu, J. Zhai, C. Yin, Y. Fan, J. Cheng, S. Liu, and Z. Shi, Theoretical prediction of high-temperature superconductivity in SrAuH_3 at ambient pressure, *Phys. Rev. B* **110**, 214504 (2024).
- [29] Y. He, J. Lu, X. Wang, and J.-j. Shi, Phonon-mediated superconductivity in the metal-bonded perovskite Al_4H up to 54K under ambient pressure, *Phys. Rev. B* **108**, 054515 (2023).
- [30] M. Du, H. Huang, Z. Zhang, M. Wang, H. Song, D. Duan, and T. Cui, High-Temperature Superconductivity in Perovskite Hydride Below 10 GPa, *Adv. Sci.* **11**, 2408370 (2024).
- [31] S. Baroni, S. De Gironcoli, A. Dal Corso, and P. Giannozzi, Phonons and related crystal properties from density-functional perturbation theory, *Rev. Mod. Phys.* **73**, 515 (2001).
- [32] N. R. Werthamer, Self-Consistent Phonon Formulation of Anharmonic Lattice Dynamics, *Phys. Rev. B* **1**, 572 (1970).
- [33] L. Monacelli, R. Bianco, M. Cherubini, M. Calandra, I. Errea, and F. Mauri, The stochastic self-consistent harmonic approximation: calculating vibrational properties of materials with full quantum and anharmonic effects, *J. Phys.: Condens. Matter* **33**, 363001 (2021).
- [34] C. Stanitski and J. Tanaka, Ternary hydrides of calcium and strontium with palladium, *J. Solid State Chem.* **4**, 331 (1972).
- [35] M. Olofsson-Mårtensson, M. Kritikos, and D. Noréus, A novel tetrahedral formally zerovalent-palladium hydrido complex stabilized by divalent alkaline earth counterions, *J. Am. Chem. Soc.* **121**, 10908 (1999).
- [36] W. Bronger and G. Ridder, Synthese und Struktur von $\text{SrPdH}_{2.7}$, *J. Alloy. Compd.* **210**, 53 (1994).
- [37] H. Yagyu, M. Kato, T. Noji, and Y. Koike, Synthesis of perovskite-type hydrides APdH_3 ($A = \text{Sr, Ba}$) by a new method using CaH_2 as a H_2 -source, *Phys. Procedia* **45**, 109 (2013).
- [38] A. Iandelli and A. Palenzona, The europium-palladium system, *J. Less-Common Met.s* **38**, 1 (1974).
- [39] P. Giannozzi, S. Baroni, N. Bonini, M. Calandra, R. Car, C. Cavazzoni, D. Ceresoli, G. L. Chiarotti, M. Cococcioni, I. Dabo, *et al.*, QUANTUM ESPRESSO: a modular and open-source software project for quantum simulations of materials, *J. Phys.: Condens. Matter* **21**, 395502 (2009).
- [40] P. Giannozzi, O. Andreussi, T. Brumme, O. Bunau, M. B. Nardelli, M. Calandra, R. Car, C. Cavazzoni, D. Ceresoli, M. Cococcioni, *et al.*, Advanced capabilities for materials modelling with QUANTUM ESPRESSO, *J. Phys.: Condens. Matter* **29**, 465901 (2017).
- [41] P. Giannozzi, O. Baseggio, P. Bonfà, D. Brunato, R. Car, I. Carnimeo, C. Cavazzoni, S. de Gironcoli, P. Delugas, F. Ferrari Ruffino, A. Ferretti, N. Marzari, I. Timrov, A. Urru, and S. Baroni, QUANTUM ESPRESSO toward the exascale, *J. Chem. Phys.* **152**, 154105 (2020).
- [42] K. F. Garrity, J. W. Bennett, K. M. Rabe, and D. Vanderbilt, Pseudopotentials for high-throughput DFT calculations, *Comput. Mater. Sci.* **81**, 446 (2014).
- [43] M. L. Evans, J. Bergsma, A. Merkys, C. W. Andersen, O. B. Andersson, D. Beltrán, E. Blokhin, T. M. Boland, R. Castañeda Balderas, K. Choudhary, A. Díaz Díaz, R. Domínguez García, H. Eckert, K. Eimre, M. E. Fuentes Montero, A. M. Krajewski, J. J. Mortensen, J. M. Nápoles Duarte, J. Pietryga, J. Qi, F. d. J. Trejo Carrillo, A. Vaitkus, J. Yu, A. Zettl, P. B. de Castro, J. Carlsson, T. F. T. Cerqueira, S. Divilov, H. Hajiyani, F. Hanke, K. Jose, C. Oses, J. Riebesell, J. Schmidt, D. Winston, C. Xie, X. Yang, S. Bonella, S. Botti, S. Curtarolo, C. Draxl, L. E. Fuentes Cobas, A. Hospital, Z.-K. Liu, M. A. L. Marques, N. Marzari, A. J. Morris, S. P. Ong, M. Orozco, K. A. Persson, K. S. Thygesen, C. Wolverton, M. Scheidgen, C. Toher, G. J. Conduit, G. Pizzi, S. Gražulis, G.-M. Rignanese, and R. Armiento, Developments and applications of the OPTIMADE API for materials discovery, design, and data exchange, *Digit. Discov.* **3**, 1509 (2024).
- [44] A. Merchant, S. Batzner, S. S. Schoenholz, M. Aykol, G. Cheon, and E. D. Cubuk, Scaling deep learning for materials discovery, *Nature* **624**, 80 (2023).
- [45] P. Hohenberg and W. Kohn, Inhomogeneous Electron Gas, *Phys. Rev.* **136**, B864 (1964).
- [46] W. Kohn and L. J. Sham, Self-Consistent Equations Including Exchange and Correlation Effects, *Phys. Rev.* **140**, A1133 (1965).
- [47] S. Baroni, S. de Gironcoli, A. Dal Corso, and P. Giannozzi, Phonons and related crystal properties from density-functional perturbation theory, *Rev. Mod. Phys.* **73**, 515 (2001).
- [48] J. P. Perdew, K. Burke, and M. Ernzerhof, Generalized Gradient Approximation Made Simple, *Phys. Rev. Lett.* **77**, 3865 (1996).
- [49] D. R. Hamann, Optimized norm-conserving Vanderbilt pseudopotentials, *Phys. Rev. B* **88**, 085117 (2013).
- [50] M. Schlipf and F. Gygi, Optimization algorithm for the generation of ONCV pseudopotentials, *Comput. Phys. Commun.* **196**, 36 (2015).
- [51] H. J. Monkhorst and J. D. Pack, Special points for Brillouin-zone integrations, *Phys. Rev. B* **13**, 5188 (1976).
- [52] B. H. Toby and R. B. Von Dreele, GSAS-II: the genesis of a modern open-source all purpose crystallography software package, *J. Appl. Crystallogr.* **46**, 544 (2013).
- [53] M. Methfessel and A. T. Paxton, High-precision sampling for Brillouin-zone integration in metals, *Phys. Rev. B* **40**, 3616 (1989).
- [54] A. V. Shapeev, Moment Tensor Potentials: A Class of Systematically Improvable Interatomic Potentials, *Multiscale Model. Sim.* **14**, 1153 (2016).
- [55] I. S. Novikov, K. Gubaev, E. V. Podryabinkin, and A. V. Shapeev, The MLIP package: moment tensor potentials

- with MPI and active learning, *Mach. Learn.: Sci. Technol.* **2**, 025002 (2020).
- [56] R. Lucrezi, E. Kogler, S. Di Cataldo, M. Aichhorn, L. Boeri, and C. Heil, Quantum lattice dynamics and their importance in ternary superhydride clathrates, *Commun. Phys.* **6**, 298 (2023).
- [57] R. Lucrezi, P. P. Ferreira, M. Aichhorn, and C. Heil, Temperature and quantum anharmonic lattice effects on stability and superconductivity in lutetium trihydride, *Nature Commun.* **15**, 441 (2024).
- [58] H. Lee, S. Poncé, K. Bushick, S. Hajinazar, J. Lafuente-Bartolome, J. Leveillee, C. Lian, J.-M. Lihm, F. Macheda, H. Mori, *et al.*, Electron-phonon physics from first principles using the EPW code, *npj Comput. Mater.* **9**, 156 (2023).
- [59] P. Ferreira, R. Lucrezi, I. Guilhon, M. Marques, L. Teles, C. Heil, and L. Eleno, Ab initio modeling of superconducting alloys, *Mater. Today Phys.* **48**, 101547 (2024).
- [60] J. Bardeen, L. N. Cooper, and J. R. Schrieffer, Theory of superconductivity, *Phys. Rev.* **108**, 1175 (1957).
- [61] R. Lucrezi, P. P. Ferreira, S. Hajinazar, H. Mori, H. Paudyal, E. R. Margine, and C. Heil, Full-bandwidth anisotropic Migdal-Eliashberg theory and its application to superhydrides, *Commun. Phys.* **7**, 33 (2024).
- [62] A. Migdal, Interaction between electrons and lattice vibrations in a normal metal, *Sov. Phys. JETP* **7**, 996 (1958).
- [63] G. Eliashberg, Interactions between electrons and lattice vibrations in a superconductor, *Sov. Phys. JETP* **11**, 696 (1960).
- [64] E. Kogler, D. Spath, R. Lucrezi, H. Mori, Z. Zhu, Z. Li, E. R. Margine, and C. Heil, IsoME: Streamlining High-Precision Eliashberg Calculations, *Comput. Phys. Commun.* , 109720 (2025).
- [65] C. Pellegrini and A. Sanna, Ab initio methods for superconductivity, *Nat. Rev. Phys.* **6** (2024).
- [66] P. B. Allen and R. C. Dynes, Transition temperature of strong-coupled superconductors reanalyzed, *Phys. Rev. B* **12**, 905 (1975).
- [67] P. Morel and P. W. Anderson, Calculation of the Superconducting State Parameters with Retarded Electron-Phonon Interaction, *Phys. Rev.* **125**, 1263 (1962).
- [68] J. Schirber and C. Northrup Jr, Concentration dependence of the superconducting transition temperature in PdHx and PdDx, *Phys. Rev. B* **10**, 3818 (1974).
- [69] I. Errea, M. Calandra, and F. Mauri, First-principles theory of anharmonicity and the inverse isotope effect in superconducting palladium-hydride compounds, *Phys. Rev. Lett.* **111**, 177002 (2013).